

On the Load Multiaxiality Effect on the Cyclic Behaviour of Magnesium Alloys

A. Gryguć, S. M. H. Karparvarfard, A. Roostaei, D. Toscano, S. Shaha, B. Behraves, and H. Jahed

Abstract

While most fatigue-related studies on wrought magnesium alloys are under uniaxial push–pull loading condition, structural members are mostly under multiaxial stresses in real-life applications. This study addresses the effect of load multiaxiality on the cyclic behaviour of several wrought magnesium alloys: AZ31B, AM30, AZ80, and ZK60 under multiaxial tension/compression–torsion loading. In particular, the influence of the presence of shear on normal stress response and vice versa is studied. In addition, phase angle effects on the stress–strain response and fatigue life are discussed. Strain energy density (SED) is introduced as a suitable fatigue damage parameter to connect and compare uniaxial and multiaxial cases. It is shown that irrespective of loading direction and/or phase angle, SED closely correlates experimental results. Beyond strain of ~ 0.4 – 0.5% , the strain-controlled cyclic behaviour in uniaxial push–pull is dominated by twinning/de-twinning, while in pure shear deformation is dominated by basal slip. The effect of each of these load directions on the other in a multiaxial loading is considered in two cases: at low axial strain amplitudes the interaction is mutual, and at high axial strain amplitudes axial strain dominates. It is believed that the re-orientation of basal planes due to twinning/de-twinning caused by axial strain favours basal slip in twinned grains resulting in better accommodation of shear strain. Further, three load phase angles of 0, 45, and 90 were considered. It is observed that the phase angle has minimal effect on life at low axial strain values; however, at higher axial strain amplitudes out-of-phase angle causes more damage. The re-orientation of matrix due to twinning and rotation of the principal axis due to

phase angle shift increase the chance of different slip/twin systems to be activated resulting in lower lives.

Keywords

Magnesium alloy • Multiaxial fatigue • Non-proportional loading • Deformation mechanism

Introduction

There is a variety of different commercially available magnesium alloys which are suitable candidates for lightweighting applications; however, they generally fall within two categories, magnesium–aluminum alloy systems and alloys which are grain refined utilizing zirconium. Those alloys which fall under the magnesium–aluminum description can be further subdivided into the AZ family (aluminum–zinc), and AM family (aluminum–manganese); whereas, the most common Mg alloy system utilizing zirconium is ZK (or zinc–zirconium). In general, aluminum is the most common alloying element, acting to improve strength, hardness, and corrosion resistance, normally at the cost of reduced ductility [1]. For structural applications, an alloying content of ~ 5 – 6% aluminum results in the best compromise of strength and ductility, thus for this particular study two varieties of alloy from the AZ family were investigated AZ31 (3% Al) and AZ80 (8% Al) [1]. Furthermore, of the AM and ZK alloy families, the commercially available AM30 and ZK60 variants were those which were selected for this particular study.

Of the wrought varieties of magnesium alloys, texture development in the microstructure resulting from the thermomechanical processing is a well-documented phenomenon. The effect of this texture evolution upon the deformation behaviour and mechanical properties of AZ31 [2–6], AZ80 [7–12], AM30 [13, 14], and ZK60 [15–17] have been explored in detail by several researchers. From a metallurgical perspective, the role of texture has implications

A. Gryguć · S. M. H. Karparvarfard · A. Roostaei · D. Toscano · S. Shaha · B. Behraves · H. Jahed (✉)
Fatigue and Stress Analysis Laboratory (FATSLab), University of Waterloo, Waterloo, ON N2L 3G1, Canada
e-mail: hamid.jahed@uwaterloo.ca

on the microstructure at both the crystallographic and grain length scales [18]. In general, processing techniques such as rolling, forging, extrusion, or equal channel angular pressing (ECAP), result in appreciable textures, characterized by irregular “elongated” grain morphologies and bi-modal grain sizes [19]. More recently, it has been well documented that these types of processing methods introduce a strong basal texture where the alignment of the crystallographic axis (*or c-axis*) is coincident to the local compressive direction (i.e., perpendicular to the working plane) [2, 8–10, 20, 21].

The cyclic response of magnesium alloys is dominated by two different deformation mechanisms, slip and twinning [2]. The way in which the activation of each of these deformation mechanisms manifests itself in the cyclic response depends strongly on the orientation of the loading direction relative to the predominant crystallographic orientation resulting in an asymmetric hysteresis [22–25]. The asymmetry in the cyclic response of wrought magnesium alloys results from the twinning/de-twinning cyclic deformation mechanism induced by the 86.3° crystal re-orientation of the basal pole during tensile twinning [2, 26].

Under strain-controlled fatigue testing, many researchers have found that the response of wrought Mg alloys is influenced by a number of factors including the magnitude, mode, and direction of the loading; however, the multiaxial effects of the loading on the cyclic response have only recently been explored in a handful of studies. Sonsino [27] made very preliminary remarks indicating that aluminum and magnesium alloys exhibited similar tendencies to steel alloys linking ductility and sensitivity to non-proportionality in multiaxial loading [27]. This current work aims to further build upon this structure–properties relationship and explore the relationship between load multiaxiality and fatigue life/cyclic behaviour of several Mg alloys of various wrought forms.

Materials and Experimental Methods

Four different wrought magnesium alloys are presented in this study, AZ31B extrusion forged at 250 °C, AM30 extrusion, AZ80 extrusion forged at 250 °C, and ZK60 extrusion forged at 250 °C. The alloys’ conditions are commercially available extrusion form and closed die precision forgings. In general, two different types of specimens were used in the experimental data presented here. Firstly, flat “dogbone” shaped specimens for the monotonic and pure axial strain-controlled tests according to the ASTM E8 and E606 standards, respectively. Secondly, hollow thin-walled tubular specimens were utilized for the pure shear and multiaxial tests according to ASTM E2207-08. All tests

were performed on an Instron biaxial tension–torsion load frame, and strain was controlled by axial or biaxial extensometer. Details regarding specimen geometries and test protocols are available within the cited literature for each alloy [3, 6, 14, 17, 28, 29].

All microstructure specimens were prepared by first hand-sanding with 600, 800, and 1200 grit SiC paper followed by polishing with 6, 3, 1, and 0.1 μ diamond paste with an oil based lubricant on imperial cloth. Finally, the samples were polished with 0.05 μ master prep colloidal silica followed by etching with acetic-picral as mentioned in [14]. Scanning electron microscope equipped with Quanta field emission gun was used to analyze microstructure.

Texture analysis was performed on the polished and etched sample using a Bruker D8-Discover equipped with an advanced 2D area detector. The experiment was conducted by measuring incomplete pole figures of {0001}, {10-10}, {10-11}, and {1-102} planes for tilt angle Ψ between 0° and 75° and in axis rotation Φ between 0° and 360° in the back reflection mode using CuK α radiation at 40 kV and 40 mA. Finally, the complete pole figures (PF) were calculated based on the measured incomplete pole figures using DIFFRAC. Suite texture software.

Table 1 contains monotonic properties and average grain size for all the chosen conditions for each alloy.

Figures 1 and 2 show the five loading paths for the fully reversed fatigue experiments. Path (a) is pure shear (γ), (b) pure axial (ϵ), (c) biaxial proportional, (d) biaxial non-proportional (45° out of phase), and (e) biaxial non-proportional (90° out of phase). In general, all the experiments were strain control exclusively during cyclic loading in the low cycle fatigue LCF (<10,000 cycles) and changed to load control in the few tests where the response stabilized, and the life exceeded this threshold. Failure criterion was a 50% drop in the peak or valley loads/torques or catastrophic failure (through crack), whichever occurs first.

Table 1 Summary of monotonic properties for various Mg alloys and processing conditions

	Condition	σ_{YS} [MPa]	σ_{UTS}	ϵ_{FAIL} [%]	Grain size [μm]
AZ31B	Forged (20 mm/s @ 250 °C) [6]	221	258	12.4	9.9
AM30	Extruded (-F) [28]	164	244	15.0	8.0–25.0
AZ80	Forged (20 mm/s @ 250 °C) [12]	286	385	15.3	10.0
ZK60	Forged (20 mm/s @ 250 °C)	281	336	15.5	5.8

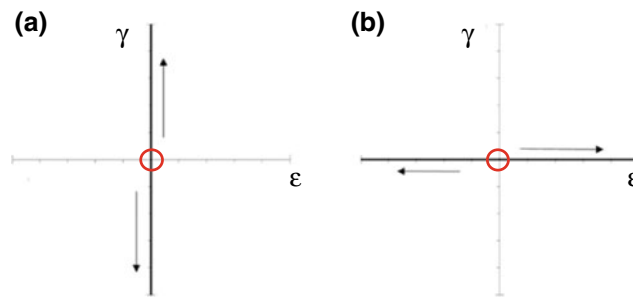


Fig. 1 Uniaxial loading paths used for fatigue experiments **a** pure shear and **b** pure axial

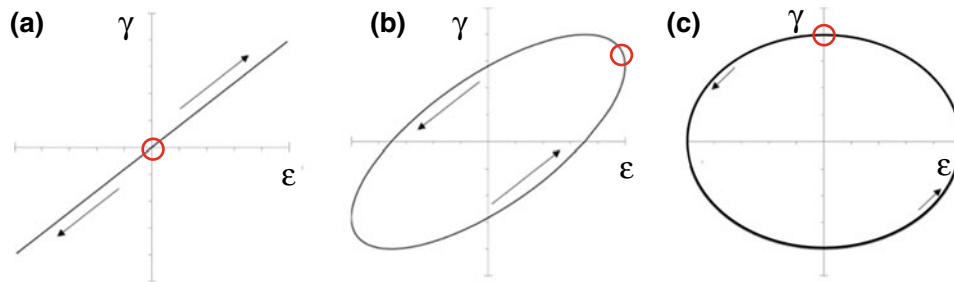


Fig. 2 Multiaxial loading paths used for fatigue experiments **c** proportional (in-phase), **d** non-proportional 45° out of phase, **e** non-proportional 90° out of phase

Results and Discussion

Low Cycle Fatigue

Figure 3 illustrates the strain life response for load path (b) and Fig. 4 for load path (a) for all alloys/conditions.

It can be observed that the difference in life for pure axial loading (path b) is less than those in pure shear in the LCF regime. Several researchers [4, 29–33] have observed a “kink” in the axial strain life curve in various wrought Mg alloys in the regime of life between 10^3 and 10^4 cycles (0.4–0.5%) which varies depending on both the strain path and alloy/processing conditions. This can be observed in most of the alloys and conditions being presented in Fig. 3 for the pure axial load path (b). This results from a change in the cyclic deformation mechanism being twinning/de-twinning activity dominating the plastic deformation at strain amplitudes above the kink point and dislocation slip below the kink point. This transitional life between cyclic deformation mechanisms coincides with a meaningful mean stress development as the strain amplitude increases [4]. In contrast, the deformation mechanism in pure shear (load path a, for shear strains $<1.5\%$) is not twinning/de-twinning dominated, and thus no distinguishable kink is observed for any of the materials as can be seen in Fig. 4. The two different deformation mechanisms in axial and shear cyclic loading are corroborated by fracture surface microstructure and the

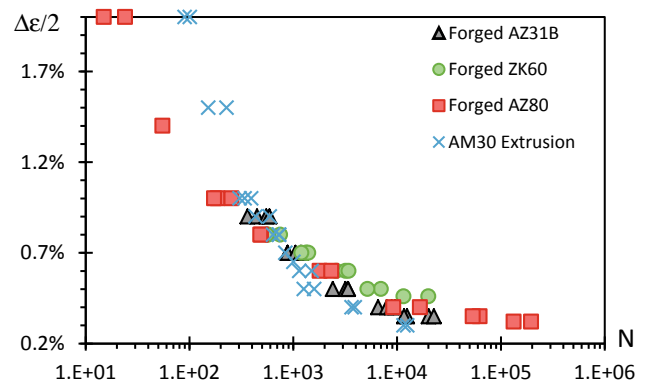


Fig. 3 ϵ - N curve for pure axial load path (b)

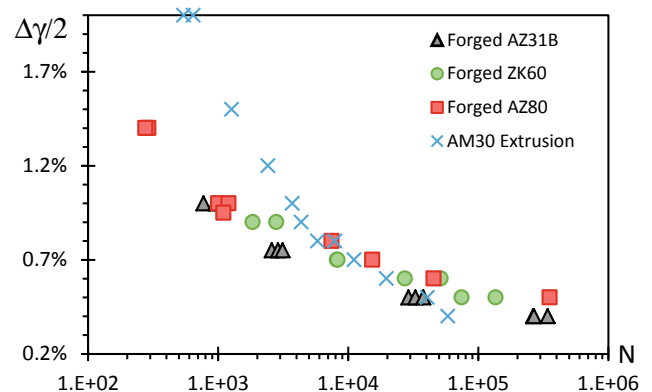


Fig. 4 γ - N curve for pure shear load path (a)

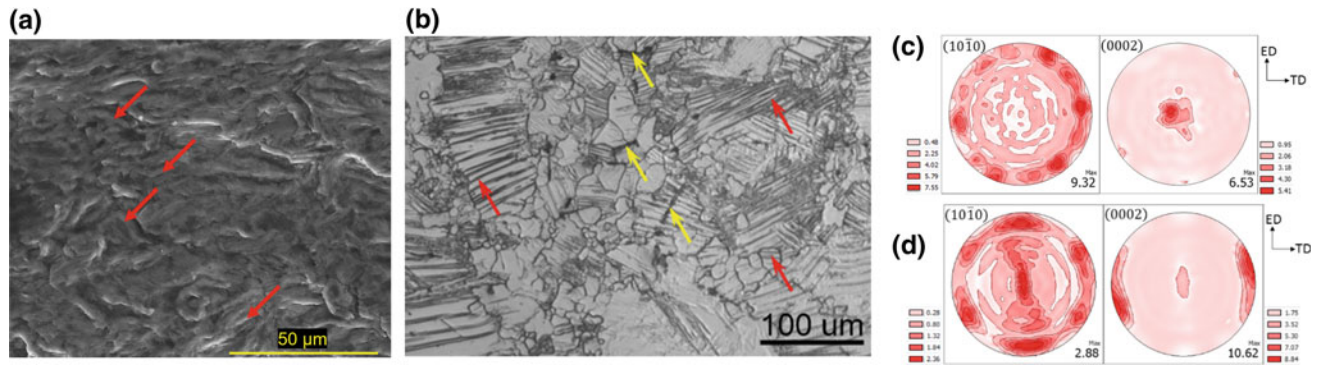


Fig. 5 SEM images of **a** the fracture surface of an AZ31B sample tested at 0.4% axial strain amplitude showing evidence of extension twin lamellae (red arrows) near the crack initiation zone, **b** near the fracture surface of sample tested at 1% with red and yellow arrows showing the residual twins and cracks observed along twin boundaries,

respectively; **(c** and **d)** pole figures of the AM30 extrusion in as-received condition and after cyclic axial strain amplitude of 2%, respectively, showing the re-orientation of basal planes (0002) due to twinning

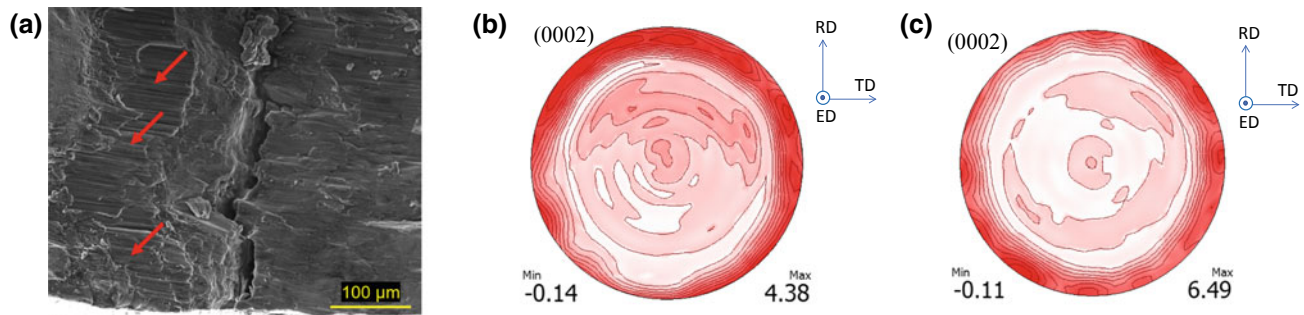


Fig. 6 SEM images of **a** the fracture surface of the primary shear crack in AZ31B tested under cyclic shear strain of 0.4% showing extensive slip bands (red arrows) surrounding significant secondary cracks;

(b and **c)** pole figures of ZK60 before and after cyclic shear of 1.1%, respectively, confirming no change in the orientation of basal planes (0002)

texture evolution as shown in Figs. 5 and 6. Figure 5 shows twin formation in axial cyclic strain, and Fig. 6 shows slip deformation in cyclic shear strain.

Energy as a Fatigue Damage Parameter

To establish a common background for comparing uniaxial and multiaxial cyclic tests, strain energy density (SED) as a measure of fatigue damage is adopted. Strain energy density has been suggested as a suitable fatigue damage parameter for variety of different materials [34–38], and particularly for wrought magnesium alloys [3, 10–12, 14, 39, 40]. Given the asymmetric and anisotropic behaviour of wrought magnesium alloys, SED has proven to be the most effective fatigue correlation parameter [14]. The total SED is implemented as a damage parameter and is constituted by its elastic and plastic components. The plastic component is defined as the area enveloped by the stabilized hysteresis loop. The elastic component which accounts for mean stress is defined as the following [41]:

$$\Delta E_e^+ = \frac{(\sigma_{\max} + \sigma_{\text{mean}})\sigma_a}{2E_{\text{cyc}}} (\text{Axial})$$

Similarly for shear, the following relationship is proposed.

$$\Delta E_e^+ = \frac{(\tau_{\max} + \tau_{\text{mean}})\tau_a}{2G_{\text{cyc}}} (\text{Shear})$$

where σ_{\max} is the maximum and σ_{mean} the mean axial stress for (path b), and τ_{\max} & τ_{mean} are the peak and mean shear stresses (path a) for the stabilized half-life response. Multiaxial cyclic tests path (c–e) was performed on AZ31B forged, AM30 extrusion, AZ80 forged, and ZK60 forged. The total SED for each test was taken as damage parameter to correlate with life. Figure 7 shows how well SED correlates fatigue data irrespective of loading path, for pure axial, pure shear, and multiaxial with any phase angle.

There are two separate effects which can be examined in biaxial responses of the various alloys and material conditions: primarily, the effect of the load multiaxiality, and secondly the effect of the level of non-proportionality or the

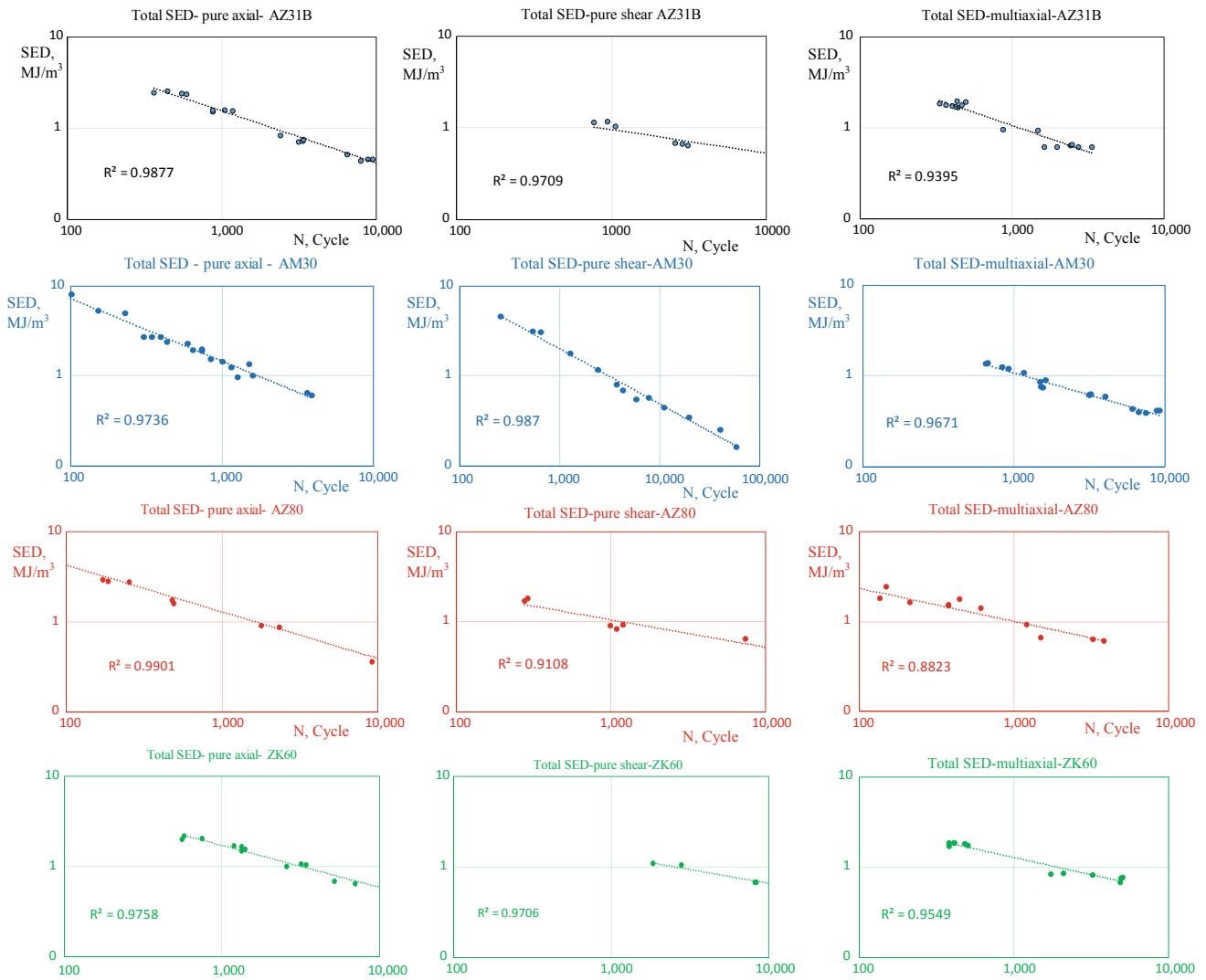


Fig. 7 Total strain energy density correlation with life in pure axial, pure shear, and multiaxial strains for AZ31B, AM30, AZ80, and ZK60 at LCF

phase angle effect. Figures 8 and 9 illustrate the relationship between axial, shear, and total SED for the investigated alloys for a variety of phase angles with a low and high proportionality ratio, respectively.

Firstly, the load axes effect in biaxial loading is considered. There exists a threshold axial strain ϵ amplitude where axial loading will begin to dominate the cyclic response and increase its proportion of total SED. This threshold corresponds with the “kink” observed in the uniaxial ϵ - N axial curve where the deformation mechanism shifts from predominantly elastic and small levels of slip-based plasticity behaviour at $\epsilon < \epsilon_{\text{kink}}$ to twinning/de-twinning behaviour at strain amplitudes $\epsilon > \epsilon_{\text{kink}}$. Below this threshold ($\epsilon < 0.4$ – 0.5%), and as depicted by Fig. 8, the share of axial SED and shear SED in total SED is the same and around $\frac{1}{2}$ of the total SED. Within this regime, the damage is equally shared by

the two axes of loading. However, for biaxial loading with axial strain higher than the threshold ($\epsilon > 0.5\%$), the axial SED becomes dominant, causing the majority of damage (e.g., close to 80% of the damage in AZ31B in Fig. 9). This is due to twinning/de-twinning caused by axial strain above the threshold. The re-orientation of basal planes due to twinning/de-twinning caused by axial strain favours basal slip in twinned grains resulting in better accommodation of shear strain. Hence, less energy is required for accommodating the shear strain as compared to the one required in the absence of axial strain. The dominance of axial strain in biaxial loading above the threshold is corroborated by the cracking mechanism. Figure 10 shows a typical macroscopic crack morphology for a failed sample under pure axial and pure shear strain path. It can be observed that the crack path morphology for pure shear loading (path a) is purely

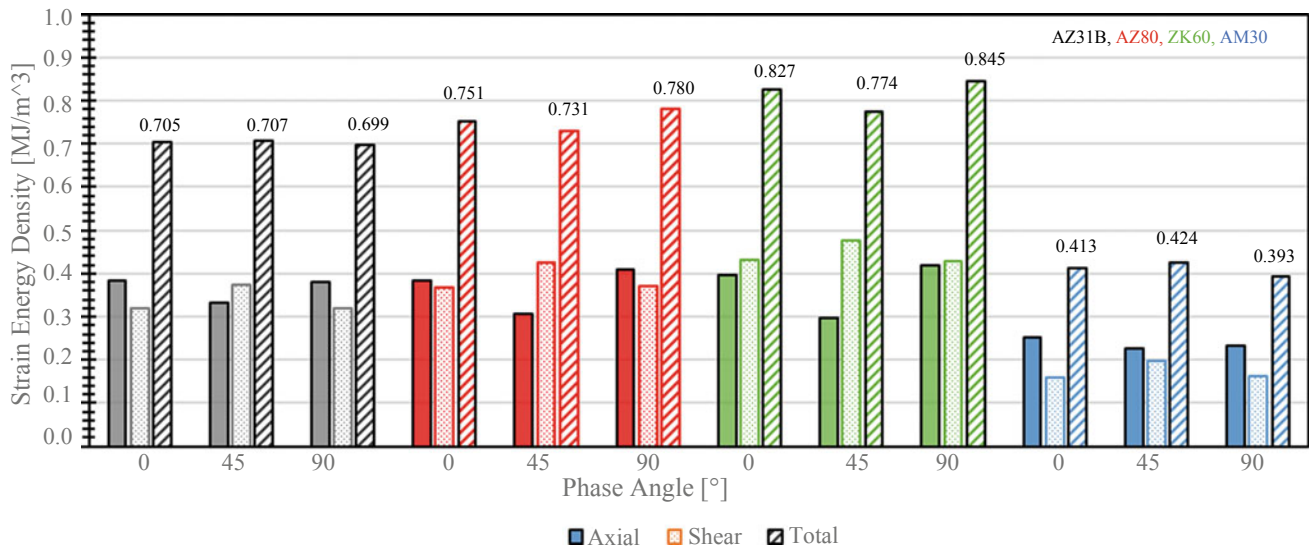


Fig. 8 Relationship between axial, shear, and total SED for the investigated alloys for a variety of phase angles and a proportionality ratio of $\epsilon/\gamma = 0.8$ and low axial strain amplitude (for B&W version note that from left to right, first three results are on AZ31B; second three results are on AZ80; third three results are on ZK60; and fourth three results are on AM30)

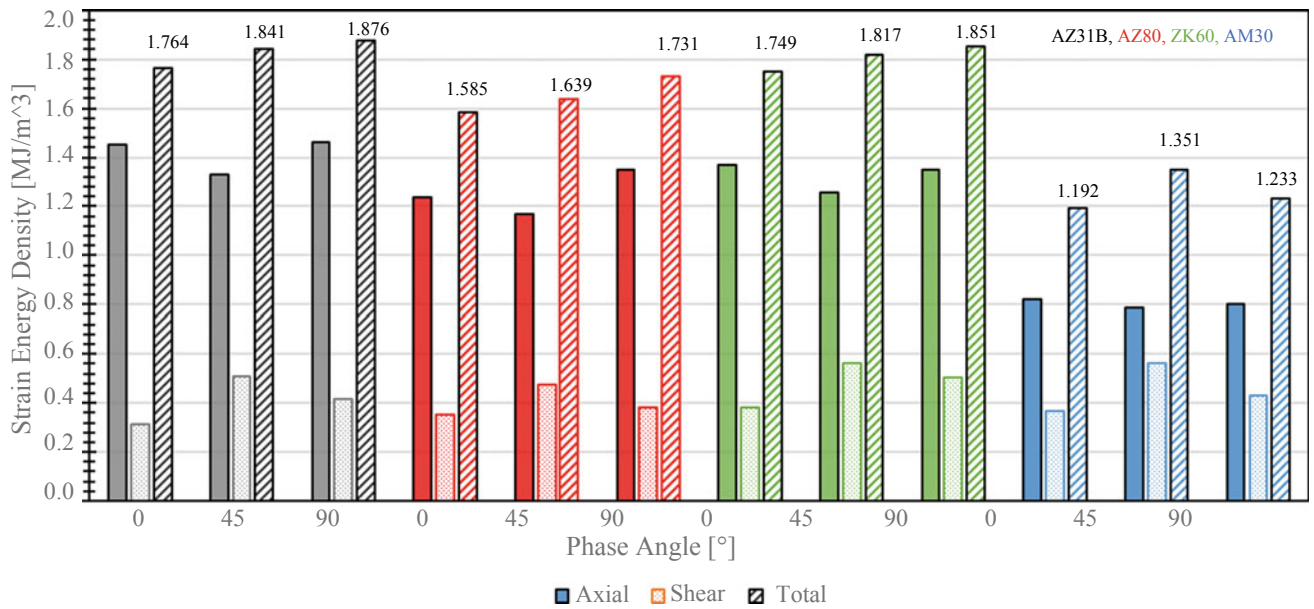
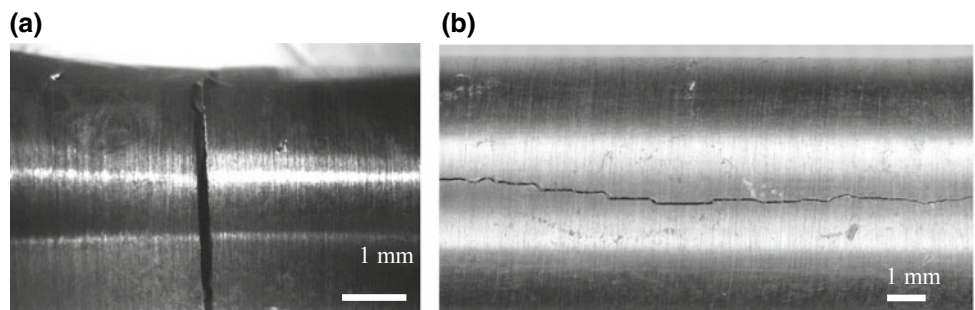


Fig. 9 Relationship between axial, shear, and total SED for the investigated alloys for a variety of phase angles and a proportionality ratio of $\epsilon/\gamma = 1.4$ with high axial strain amplitude (for B&W version note that from left to right, first three results are on AZ31B; second three results are on AZ80; third three results are on ZK60; and fourth three results are on AM30)

Fig. 10 Macroscopic fracture morphology for an AZ80 failed sample under **a** pure axial **b** pure shear strain



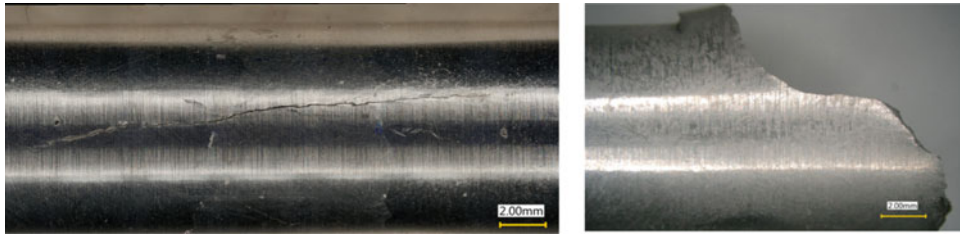


Fig. 11 Macroscopic fracture morphology for a ZK60 failure **a** under 0.3% axial and 0.7% shear strain showing longitudinal crack, **b** under 0.6% axial and 0.7% shear strain showing transverse crack

longitudinal (aligned with the tubular specimen axis) while crack path for pure axial strain (path b) is transverse. In biaxial loading however, as depicted by Fig. 11, when the axial strain is above the threshold, the cracking is always transverse (Fig. 11b), irrespective of the level of shear strain amplitude. On the other hand, when the axial strain is below threshold (Fig. 11a) and shear strain is large, the cracking is longitudinal, confirming low influence of axial strain on final failure.

With regards to the sensitivity to the level of non-proportionality or phase angle effect, a few observations can be made. As depicted by Fig. 8, at low value of axial strain, there seems to be no effect of phase angle on total SED. This is clearly seen in the case of AZ31B for $\varepsilon = 0.4\%$ and $\gamma = 0.5\%$ where the total SED independent of the phase angle in all three cases is 0.7 MJ/m^3 . For AZ80 and ZK60 at the same biaxial loading, the maximum difference of SED with respect to phase angles 0, 45, and 90 is 6% and 7%, respectively. This difference for AM30 biaxial loading with $\varepsilon = 0.3\%$ and $\gamma = 0.4\%$ is only 7%. However, at high axial strain values, as depicted by Fig. 9, the phase angle changes the total SED. For AZ31B, AZ80, and ZK60 biaxial loading with $\varepsilon = 0.7\%$ and $\gamma = 0.5\%$, the SED increases (life decreases) as phase angle increases. For AM30 with lower biaxial loading of $\varepsilon = 0.5\%$ and $\gamma = 0.6\%$, again the effect of load angle is visible. Xiong et al. [4] observed that in extruded AZ31B non-proportional loading results in a higher population of grains experiencing twinning/de-twinning as well as easier activation of various sets of twins AZ31B. These deformation induced twins can serve as sites for crack initiation which can potentially have a detrimental effect on fatigue life. Furthermore, the additional non-proportional hardening that can be induced by the rotation of the principal axis can also lead to higher cyclic energies and has the effect of further reducing the fatigue life [37]. The AM30 alloy behaved somewhat different, with longer life occurring at 90° than at 45° , due to the attenuation of the cyclic hardening in the axial direction under non-proportional loading, a phenomenon that as was observed by Roostaei and Jahed [29]. The variation in SED in all alloys at high biaxial strain amplitudes in Fig. 9 remains small and less than 12%. While

rotation of principal axes in out-of-phase loading accommodates more deformation mechanisms to occur, however, limited number of slip systems in magnesium alloys limits its detrimental effect [42].

Conclusion

The effect of multiaxiality on the cyclic behaviour was studied for several Mg alloys of the extrusion and forge variety. Several different loading paths were presented, uniaxial and biaxial, with varying levels of non-proportionality. Based upon the results, the following conclusions can be drawn:

1. A distinct kink in the ε - N response under pure axial loading for all the presented materials represents a fundamental shift in the cyclic deformation mechanism. This kink is associated with the onset of domination of twinning/de-twinning in materials response in uniaxial and biaxial loadings. No such kink is observed in the pure shear ε - N response which is dominated by slip.
2. Strain energy density (SED) correlates all fatigue experimental results irrespective of the axes of loading.
3. Under multiaxial loading, at strain amplitudes above a certain “kink” threshold when sufficient plasticity is induced, the axial component tends to dominate the biaxial loading. Below this threshold, the sensitivity of the response to the relative intensity of each loading axis as well as the phase angle is quite low.
4. Under non-proportional loading, if the rotation of the principal axis causes the axial proportion of total SED to increase, it results in a lower fatigue life, and this was observed in AZ31, AZ80, and ZK60 alloys.
5. In the tubular specimens utilized, the crack path behaviour is characterized by transverse cracking (tensile type failure) for the majority of strain paths. The only exceptions to this are the pure shear load path which exhibited longitudinal cracking in the LCF regime and helical cracking (45°) in the HCF.
6. Under multiaxial loading, fatigue cracks normally initiate at the surface of the tubular sample regardless of the

relative magnitudes of each strain component. In general, this was true for all alloys and material conditions investigated.

7. The transverse cracking path was relatively insensitive to the level of non-proportionality of the loading.

Acknowledgements The authors would like to gratefully acknowledge the financial support of the Natural Sciences and Engineering Research Council of Canada (NSERC), Automotive Partnership Canada (APC) program under APCPJ 459269–13 grant with contributions from Multimatic Technical Centre, Ford Motor Company, and Centerline Windsor.

References

1. B. R. Powell, P. E. Krajewski, and A. A. Luo, "Magnesium alloys for lightweight powertrains and automotive structures," *Mater. Des. Manuf. Light. Veh.*, pp. 114–173, 2010.
2. L. Wu *et al.*, "Twinning-detwinning behavior during the strain-controlled low-cycle fatigue testing of a wrought magnesium alloy, ZK60A," *Acta Mater.*, vol. 56, no. 4, pp. 688–695, 2008.
3. J. Albinmoussa, H. Jahed, and S. Lambert, "Cyclic axial and cyclic torsional behaviour of extruded AZ31B magnesium alloy," *Int. J. Fatigue*, vol. 33, no. 11, pp. 1403–1416, 2011.
4. Y. Xiong, Q. Yu, and Y. Jiang, "Multiaxial fatigue of extruded AZ31B magnesium alloy," *Mater. Sci. Eng. A*, vol. 546, pp. 119–128, 2012.
5. D. Toscano, S. K. Shaha, B. Behraves, H. Jahed, and B. Williams, "Effect of forging on the low cycle fatigue behavior of cast AZ31B alloy," *Mater. Sci. Eng. A*, vol. 706, no. August, pp. 342–356, 2017.
6. D. Toscano, S. K. Shaha, B. Behraves, H. Jahed, and B. Williams, "Multiaxial Cyclic Response of Low Temperature Closed-Die Forged AZ31B Mg Alloy," *Miner. Met. Mater. Ser.*, pp. 289–296, 2019.
7. A. Gryguc, H. Jahed, B. Williams, and J. McKinley, "Magforge—Mechanical behaviour of forged AZ31B extruded magnesium in monotonic compression," *Mater. Sci. Forum*, vol. 828–829, pp. 291–297, 2015.
8. A. Gryguc, S. K. Shaha, H. Jahed, M. Wells, B. Williams, and J. McKinley, "Tensile and fatigue behaviour of as-forged AZ31B extrusion," *Frat. ed Integrita Strutt.*, vol. 10, no. 38, pp. 251–258, 2016.
9. A. Gryguc, S. K. Shaha, S. B. Behraves, H. Jahed, M. Wells, and B. Williams, "Compression Behaviour of Semi-Closed Die Forged AZ80 Extrusion," *Charact. Miner. Met. Mater. 2017*, pp. 361–369, 2017.
10. A. Gryguc *et al.*, "Monotonic and cyclic behaviour of cast and cast-forged AZ80 Mg," *Int. J. Fatigue*, vol. 104, pp. 136–149, 2017.
11. A. Gryguc *et al.*, "Low-cycle fatigue characterization and texture induced ratcheting behaviour of forged AZ80 Mg alloys," *Int. J. Fatigue*, vol. 116, pp. 429–438, 2018.
12. A. Gryguc *et al.*, "Multiaxial cyclic behaviour of extruded and forged AZ80 Mg alloy," *Int. J. Fatigue*, vol. 127, pp. 324–337, 2019.
13. A. A. Roostaei and H. Jahed, "A cyclic small-strain plasticity model for wrought Mg alloys under multiaxial loading: Numerical implementation and validation," *Int. J. Mech. Sci.*, vol. 145, no. July, pp. 318–329, 2018.
14. A. A. Roostaei and H. Jahed, "Role of loading direction on cyclic behaviour characteristics of AM30 extrusion and its fatigue damage modelling," *Mater. Sci. Eng. A*, vol. 670, pp. 26–40, 2016.
15. Y. Xiong and Y. Jiang, "Fatigue of ZK60 magnesium alloy under uniaxial loading," *Int. J. Fatigue*, vol. 64, pp. 74–83, 2014.
16. S. M. H. Karparvarfard, S. K. Shaha, S. B. Behraves, H. Jahed, and B. Williams, "12th International Fatigue Congress (FATIGUE 2018), MATEC Web of Conferences 165, 06009, 2018.
17. S. M. H. Karparvarfard, S. K. Shaha, S. B. Behraves, H. Jahed, and B. W. Williams, "Fatigue characteristics and modeling of cast and cast-forged ZK60 magnesium alloy," *Int. J. Fatigue*, vol. 118, no. November 2017, pp. 282–297, 2019.
18. J. Albinmoussa, M. J. Adinoyi, and N. Merah, "Multiaxial fatigue of extruded ZK60 magnesium alloy," *Fatigue Fract. Eng. Mater. Struct.*, no. May, pp. 1–14, 2019.
19. F. Nový, M. Janeček, V. Škorik, J. Muller, and L. Wagner, "Very high cycle fatigue behaviour of as-extruded AZ31, AZ80, and ZK60 magnesium alloys," *Int. J. Mater. Res.*, vol. 100, no. 3, pp. 288–291, 2009.
20. S. Kleiner and P. J. Uggowitzer, "Mechanical anisotropy of extruded Mg-6% Al-1% Zn alloy," *Mater. Sci. Eng. A*, vol. 379, no. 1–2, pp. 258–263, 2004.
21. X. Y. Lou, M. Li, R. K. Boger, S. R. Agnew, and R. H. Wagoner, "Hardening evolution of AZ31B Mg sheet," *Int. J. Plast.*, vol. 23, no. 1, pp. 44–86, 2007.
22. L. Wu *et al.*, "Internal stress relaxation and load redistribution during the twinning-detwinning-dominated cyclic deformation of a wrought magnesium alloy, ZK60A," *Acta Mater.*, vol. 56, no. 14, pp. 3699–3707, 2008.
23. S. Dong *et al.*, "Characteristic cyclic plastic deformation in ZK60 magnesium alloy," *Int. J. Plast.*, vol. 91, pp. 25–47, 2017.
24. S. Dong, Y. Jiang, J. Dong, F. Wang, and W. Ding, "Cyclic deformation and fatigue of extruded ZK60 magnesium alloy with aging effects," *Mater. Sci. Eng. A*, vol. 615, pp. 262–272, 2014.
25. Q. Yu, J. Zhang, Y. Jiang, and Q. Li, "An experimental study on cyclic deformation and fatigue of extruded ZK60 magnesium alloy," *Int. J. Fatigue*, vol. 36, no. 1, pp. 47–58, 2012.
26. M. G. Jiang, H. Yan, and R. S. Chen, "Twinning, recrystallization and texture development during multi-directional impact forging in an AZ61 Mg alloy," *J. Alloys Compd.*, vol. 650, pp. 399–409, 2015.
27. C. M. Sonsino, "Material Influence on Multiaxial Fatigue Response," ICMFF9 proceedings, pp. 41–57.
28. J. Albinmoussa *et al.*, "Monotonic and fatigue behavior of magnesium extrusion alloy AM30: An international benchmark test in the 'magnesium Front End Research and Development Project,'" *SAE Tech. Pap.*, vol. 9781118858, pp. 557–562, 2010.
29. A. A. Roostaei and H. Jahed, "Multiaxial cyclic behaviour and fatigue modelling of AM30 Mg alloy extrusion," *Int. J. Fatigue*, vol. 97, pp. 150–161, 2017.
30. Q. Yu, J. Zhang, Y. Jiang, and Q. Li, "Multiaxial fatigue of extruded AZ61A magnesium alloy," *Int. J. Fatigue*, vol. 33, no. 3, pp. 437–447, 2011.
31. F. Castro and Y. Jiang, "Fatigue life and early cracking predictions of extruded AZ31B magnesium alloy using critical plane approaches," *Int. J. Fatigue*, vol. 88, pp. 236–246, 2016.
32. Y. Xiong and Y. Jiang, "Cyclic deformation and fatigue of rolled AZ80 magnesium alloy along different material orientations," *Mater. Sci. Eng. A*, vol. 667, pp. 58–67, 2016.
33. Y. Xiong, Q. Yu, and Y. Jiang, "Cyclic deformation and fatigue of extruded AZ31B magnesium alloy under different strain ratios," *Mater. Sci. Eng. A*, vol. 649, pp. 93–103, 2016.

34. Golos K, Ellyin F. A total strain energy density theory for cumulative fatigue damage. *J Pressure Vessel Technol*;110:36–41,1988.
35. H. Jahed and A. Varvani-Farahani, “Upper and lower fatigue life limits model using energy-based fatigue properties,” *Int. J. Fatigue*, vol. 28, no. 5–6, pp. 467–473, 2006.
36. Jahed H, Varvani A, Noban M, Khalaji I, An energy-based fatigue life assessment model for various metallic materials under proportional and non-proportional loading conditions, *International Journal of Fatigue*, 2007, 29(4), 647–655.
37. Noban M, Jahed H, Ibrahim E, Ince A, Load path sensitivity and fatigue life estimation of 30CrNiMo8HH, *International Journal of Fatigue*, 2012, 37, 123–133.
38. Noban M, Jahed H, Winkler S, Ince A, Fatigue characterization and modeling of 30CrNiMo8HH under multiaxial loading, *Materials Science and Engineering A*, 2011, 528(6), 2484–2494.
39. S. H. Park, S. G. Hong, B. H. Lee, W. Bang and C. S. Lee, “Low-cycle fatigue characteristics of rolled Mg–3Al–1Zn alloy,” *International Journal of Fatigue*, vol. 32, pp. 1835–1842, 2010.
40. H. Jahed and J. Albinmousa, “Multiaxial behaviour of wrought magnesium alloys - A review and suitability of energy-based fatigue life model,” *Theor. Appl. Fract. Mech.*, vol. 73, pp. 97–108, 2014.
41. A. A. Roostaei, A. Pahlevanpour, S. B. Behraves, and H. Jahed, “On the definition of elastic strain energy density in fatigue modelling,” *Int. J. Fatigue*, vol. 121, no. December 2018, pp. 237–242, 2019.
42. D. Skibicki and Ł. Pejkowski, “The relationship between additional non-proportional hardening coefficient and fatigue life,” *Int. J. Fatigue*, vol. 123, no. February, pp. 66–78, 2019.